Journal of Cleaner Production, Volume 384, January 2023, Article number 135579
DOI:10.1016/j.jclepro.2022.135579

Highly robust Zr-stabilized CaO nanoadsorbent developed by a facile one-pot MWCNT-assistance method for CO_2 capture under realistic calcium looping conditions

Seyed Borhan Mousavi[a], Mohammad Heidari[b,c], Farhad Rahmani[b1], Rojiar Akbari Sene[b], Peter T. Clough[d], Serap Ozmen[d]

[a] J. Mike Walker '66 Mechanical Engineering Department, Texas A&M University, College Station, TX, USA

[b] Department of Chemical Engineering, Faculty of Engineering, University of Kurdistan, Sanandaj, P.O.Box 66177-15175, Iran

[c] Faculty of Chemical & Petroleum Engineering, University of Tabriz, Tabriz, Iran

[d] Energy and Power Theme, Cranfield University, Cranfield, Bedfordshire, MK43 0AL, United Kingdom

Abstract:

This research assessed the textural and structural characterizations and CO_2 capture activity of novel and highly thermal-resistance CaO/$CaZrO_3$ adsorbents templated with MWCNT, developed via a facile one-pot preparation. Various MWCNT contents, 2.5, 5, and 10 wt.%, were incorporated into the CaO adsorbent containing 18.5 wt.% $CaZrO_3$ species characterized by XRD. The conducted structural properties revealed that the CaO grain size, BET surface area, and BJH pore volume of untemplated ZrO_2-supported CaO improved by 33.25%, 185%, and 141% through merging with 10 wt.% MWCNT, conformed with FESEM images that showed the highly porous structure. Moreover, the TGA analyses under the severe calcium looping conditions, carbonation under 15 vol.% CO_2 balanced with N_2 at 650°C for 10 min, and calcination under 100 vol.% CO_2 at 930°C for 10 min, demonstrated the incorporation of 10 wt.% MWCNT into the $CaZrO_3$-containing CaO adsorbent increased cyclic durability and the ultimate CO_2 capture capacity from 29.5% and 0.03 g CO_2/g adsorbent to 61.12% and 0.1 g CO_2/g adsorbent, indicating 107% and 233.3% enhancement, respectively. In addition to the significant reduction in CaO grain size and the formation of more high-volume pores, the influence of the MWCNT on $CaZrO_3$ distribution into the CaO structure, mitigating CaO

[1] Corresponding author.
Email address: F.rahmanichiyane@uok.ac.ir

sintering and the agglomeration of CaO grains is another potential reason for the discussed multicyclic and textural improvements. The acquired findings indicated the effectiveness of MWCNT on textural, structural, and multicyclic properties of nano-scale CaO adsorbents by forming more inner porous zones.

Keywords: CO_2 capture; calcium looping; $CaZrO_3$-containing CaO adsorbent; MWCNTs; MWCNT-templated CaO adsorbent; Chemical modification.

Nomenclature	
MWCNT	Multi-Walled Carbon Nanotube
MOF	Metal Organic Framework
LDH	Layered Double Hydroxide
XRD	X-Ray Diffraction
BET	Brunauer–Emmett–Teller
BJH	Barrett-Joyner-Halenda
FESEM	Field-Emission Scanning Electron Microscopy
EDX	Energy Dispersive X-Ray
ICP-OES	Inductively Coupled Plasma Optical Emission Spectroscopy
TGA	Thermogravimetric Analysis
CCS	Carbon Capture and Storage
CaL	Calcium Looping
D_{avg}	Average CaO crystallite size (nm)
MW	Mega Watt
ppm	Parts Per Million
C_n	CO_2 capture capacity at n^{th} cycle (g of captured CO_2/g of adsorbent)
M_n	Mass of adsorbents at the end of n^{th} carbonation step (g)
M_0	Mass of adsorbents before starting the 1^{st} carbonation step (g)
D	Cyclic durability (%)
T	Total amount of captured CO_2 (g of captured CO_2/g of adsorbent)
λ	The radiation wavelength (nm)
θ	The considered XRD peak angular position (°)
β	The total breadth at mid of the considered XRD peak (radians)

1. Introduction:

The detrimental consequences of anthropogenic climate change, such as demolishing ecosystems, floods, shortage of potable water, and droughts, have challenged human society [1-3]. The overuse of fossil fuel, the world's principal energy supply, has been conducive to raising atmospheric CO_2 emissions, identified as the central cause of global warming in recent decades [4]. According to recently conducted studies, the atmospheric CO_2 concentration has risen from 400 ppm in 2016 to 416.47 ppm in May 2020 and will pass 500 ppm by 2050 [5]. One of the primary resources of CO_2 emission is coal combustion in power plants. In this regard, a 500 MW coal-fired power plant has consistently released out *ca.* 3 Mtons CO_2 per year [6]. Carbon Capture and Storage (CCS) from industrial plants have been proposed as a promising scenario to alleviate atmospheric CO_2 emission via three disparate-mechanism approaches, namely pre-, oxy-, and post-combustion [7]. Notwithstanding the low CO_2 concentration of discharged flue gas from main sources for the post-combustion method, generally less than 15%, this approach has been regarded as the most competitive in cost and feasibility to integrate with the flue gas purification technology [8]. In comparison with applicable post-combustion methods, such as amine scrubbing absorption, membrane, cryogenic, and ionic liquids [9], solid adsorbents have been considered novel strategies owing to their remarkable capability to capture CO_2 in a wide temperature range of 20-700℃ with high sorption capacity [10]. There are a host of useful solid adsorbents that can capture CO_2 from released flue gas in low temperatures, <200℃, intermediate temperature, between 200-400 ℃, and high temperatures, >400℃. Carbon-based materials, MOF, zeolite, alkali metal carbonates, and copolymers are identified as low-temperatures adsorbents, LDH and MgO have great capacities to capture CO_2 at intermediate temperature, and lithium silicates, lithium zirconates, and CaO captured considerable amounts of CO_2 at high temperatures [11-15]. Among the mentioned solid adsorbents, CaO-based adsorbents have demonstrated high CO_2 capture capacity via CaL process. Considering the significant benefits of CaO adsorbents, such as CO_2 adsorption at high temperatures, fast kinetics of adsorption reaction, and wide availability of cost-effective CaO resources, numerous studies have been conducted on CO_2 adsorption via CaO-based adsorbents [16]. For the first of knowledge, Shimizu et al. [17] proposed the novel CaL technology for CO_2 adsorption from released flue gas via the reversible gas-solid reaction of carbonation/calcination cyclic of CaO adsorbents using twin inter-connected fluidized bed reactors. CaO-based adsorbents have demonstrated the remarkable cyclic CO_2 capture potential according to Eqs (1) and (2) [16]:

$CaO(s) + CO_2(g) \rightarrow CaCO_3(s)$ $\Delta H_r^0 = -178$ kJ/mol (Carbonation) (1)

$CaCO_3(s) \rightarrow CaO(s) + CO_2(g)$ $\Delta H_r^0 = +178$ kJ/mol (Calcination) (2)

According to Eq. (1), the extent of CO_2 emitted by inlet flue gases, containing 10-15 vol.% CO_2, is partially captured by CaO adsorbent at temperatures ranging over 600-700°C, leading to the partial formation of $CaCO_3$. Afterward, CaO is regenerated by the calcination of circulated $CaCO_3$ from the carbonator at temperatures above 850°C, either via exterior fuel combustion or combusting fuel of pure O_2 stream [18]. The next cycle of the process commences by feeding the regenerated CaO back into the carbonator.

Despite the many advantages of CaL technology, the CO_2 capture capacity of CaO-based adsorbents gradually decreases over carbonation/calcination cycles [19]. The mentioned drawback is originated from the severe $CaCO_3$ sintering at high-temperature calcination because of the low Tamman temperature of $CaCO_3$ (~529°C), which forms a ~100 nm layer of $CaCO_3$ on the CaO surface and consequently, decreases the accessible CaO grains to adsorb CO_2 molecules [20]. As recentely published papers on nanocomposites have indicated the thermal durability of metal oxides [21-24], to overcome the particles' agglomeration, CaO particles have been structurally doped with thermal-resistance materials such as metal oxides [21-23], leading to significant improvement in thermal stability and sorption capacity [25-28]. The textural modification of nano-size adsorbents has been broadly investigated to hamper the agglomeration of nanoparticles [29-35]. Extensive studies have indicated the higher enhancement in the CO_2 adsorption capacity of modified CaO by using ZrO_2 as the promoter compared to other metal oxides [36]. Radfarnia et al. [37] demonstrated the superior performance of $CaZrO_3$ in enhancing the sorption activity of pure CaO under severe CaL conditions compared to $Ca_9Al_6O_{18}$ and MgO. In a research conducted by Antzara et al. [38], they reported 71.5% durability after 100 multiple carbonation/calcination cycles under harsh calcination conditions, including under 100 vol.% CO_2 for 5 min at 950 °C, for ZrO_2-supported CaO adsorbent prepared via sol-gel combustion synthesis method. In contrast, the sorption stability of 45.7% was reported for the Al_2O_3-supported CaO adsorbent. The substantial outcomes of lately conducted investigations on the CO_2 adsorption potential of ZrO_2-doped CaO-based adsorbents are summarized in Table 1.

In another aspect of boosting the cyclic activity of CaO-based materials, increasing the porosity of CaO texture has been identified as an integral approach to boost the CO_2 uptake capacity of CaO-based adsorbents [39]. One of the promising procedures to enhance the

porosity of CaO is the utilization of flammable bio-templates, such as lycopodium powder, microalgae, bamboo, maple leaves, polymeric microspheres, and cellulose [40-43]. The combustion of the embedded bio-templates into CaO texture creates many inner pores and raises its porosity. Naeem et al. [44] reported the effectiveness of the carbon-based templates, namely xylose and glucose, on hydrothermally developed MgO-supported CaO adsorbents, in which the hydrothermal-based developed MgO-CaO adsorbents presented ~ 2.4 and 2.3 times higher CO_2 capture capacity at 10^{th} cycle by using xylose and glucose, respectively, compared to the carbon-free hydrothermally prepared counterpart. Additionally, based on the cyclic results, the co-incorporation of MgO as promoter and xylose as template resulted in the sorption capacity of ~ 0.63 g CO_2/g adsorbent at the 10^{th} cycle, while the sorption capacity of ~ 0.18 and ~ 0.15 were recorded for mechanically mixed MgO-CaO adsorbent and limestone, respectively. Armutlulu et al. [45] utilized a substantial template-assisted hydrothermal synthesis method to prepare multishelled CaO microspheres. Templated with glucose and urea, the average CO_2 capture capacity of CaO sorbents over 10 multiple CaL cycles was enhanced by 164.3%. In the case of Al-promoted CaO microspheres, the preparation through the abovementioned templates resulted in a 156.7% increase in the average CO_2 capture capacity. In another study that employed a template-assistance preparation method, Kim et al. [46] assessed the influence of the inverse opal (IO)-like hydrothermally carbon-nanospheres-templated synthesis route on multicyclic uptake potential of pure and $Ca_3Al_2O_6$-containing CaO-based adsorbents under realistic CaL conditions. With the CaO having incorporated with $Ca_3Al_2O_6$ through the templated-assisted method using carbon nanospheres at the size of 300 nm, 337.6% and 325% enhancements in CO_2 capture durability and capacity at the ultimate cycles were recorded during 30 cycles CaL process.

Despite the abovementioned advantages of Zr-based additive, the ZrO_2-containing materials suffer from several drawbacks, including the high cost of Zr-based precursors [47, 48], the pore obstruction and non-uniform distribution of $CaZrO_3$ in the presence of high $CaZrO_3$ content, and significant reduction in accessible CaO particles by increasing the Zr-based additive due to reaction with ZrO_2 in $CaZrO_3$ formation reaction [19, 49]. The abovementioned deficiencies compel the researchers to utilize the ZrO_2-based additive in minor contents. On the other hand, it has been reported in these investigations that the thermal-stability feature of CaO-adsorbents and the amount of active CaO sites gradually decrease by reducing ZrO_2 value. Activating CaO-based adsorbents stabilized with minor ZrO_2-based additive through feasible strategies has been maintained as an unsolved challenge.

Considering the conducted literature review, most investigations revealed that the modification of CaO with ZrO_2-based metal oxide and incorporating biomass materials into CaO precursors positively improve CO_2 uptake activity and textural characterization. To the best of our knowledge, no research have focused on boosting the structural properties of CaO adsorbents modified with low ZrO_2 content using minor concentrations of auxiliary additives. Moreover, the influence of template-assistance additives on ZrO_2-supported CaO adsorbents has not been analyzed. In addition, no consideration has been paid to evaluate the influence of MWCNT additive on metal-promoted CaO nano-adsorbent.

Herein, for the first time, the highly robust MWCNT-templated $CaZrO_3$-incorporated CaO adsorbents were developed via the one-pot MWCNT-assistance synthesis method to improve the sorption activity of $CaZrO_3$-stabilized CaO adsorbent. Considering the usage of minor concentrations of ZrO_2 and MWCNT in developing adsorbents, it can be acclaimed that the novel adsorbent is highly cost-effective due to its outstanding textural and CO_2 adsorptive characteristics. The novel MWCNT-templated $CaZrO_3$-containing CaO adsorbents were prepared via a facile one-pot MWCNT-assistance synthesis method to enhance thermal durability and improve textural and structural features of CaO-based adsorbents during CO_2 capture under severe CaL conditions by using the optimum amount of additives. Therefore, the $CaZrO_3$-stabilized CaO adsorbent was doped with different MWCNT concentrations of 2.5, 5, and 10 wt.%, considering the Ca/Zr molar ratio of 15/1 and the minor content of ZrO_2.

Table 1: Summary of recent literature's activity and CaL conditions of the ZrO_2-promoted CaO adsorbents analyzed under multiple carbonation/calcination cycles.

CaO precursor		Additive precursor	Formed supports		Synthesis method	Carbonation conditions			Calcination conditions			Number of cycles	SP of the best sample (g CO_2/g adsorbent)		Substantial outcome	Refs
Precursor	CaO content (wt.%)		support	content wt.%		T (°C)	environment	t (min)	T (°C)	environment	t (min)		initial	final		
													Deactivation%			
$Ca(OH)_2$ Calcium hydroxide	73.8	$C_{12}H_{28}O_4Zr$ zirconium (IV) propoxide	$CaZrO_3$	26.2	Sol–gel	800	50% CO_2	5	800	100% N_2	~15	90	0.46	0.34	The ultimate SP of the modified sample exceeded that of reference limestone by 161.5%.	[50]
													26.1			
$Ca(NO_3)_2.4H_2O$ Calcium nitrate tetrahydrate	99.7	$ZrO(NO_3)_2 \cdot 5H_2O$ zirconium nitrate pentahydrate	$CaZrO_3$	0.3	Urea hydrolysis (using colloidal carbon spheres)	650	50% CO_2	30	850	100% N_2	10	100	0.53	0.36	The co-adsorption using a colloidal carbon sphere assists in the highest SP activity at the minimum content of the Zr additive.	[51]
													32.07			
$Ca(NO_3)_2.4H_2O$ Calcium nitrate tetrahydrate	90	$ZrO(NO_3)_2 \cdot xH_2O$ zirconium nitrate	$CaZrO_3$	10	Sol–gel	650	100% CO_2	60	780	100% N_2	60	10	0.72	0.68	The ultimate SP of sol-gel-derived CaO increased by 88.9% by doping with ZrO_2.	[52]
													5.6			
$Ca(OH)_2$ Calcium hydroxide	70	$ZrO(NO_3)_2 \cdot xH_2O$ zirconium nitrate	$CaZrO_3$	30	a wet chemical route	650	100% CO_2	5	950	100% CO_2	0	30	0.36	0.31	Raising CaZrO3 content (from 10 to 30) has no impact on ultimate SP.	[53]
													13.88			
$Ca(NO_3)_2.4H_2O$ Calcium nitrate tetrahydrate	66	$ZrO(NO_3)_2 \cdot xH_2O$ zirconium nitrate	$CaZrO_3$	34	Sol-gel	650	10% CO_2	-	920	80% CO_2	-	20	0.44	0.31	The modified sample's ultimate SP exceeds that of reference limestone by 406%.	[54]
													29.54			
$Ca(CH_3COO)_2 \cdot xH_2O$ Calcium acetate hydrate	80	$Zr(NO_3)_4 \cdot xH_2O$ zirconium nitrate	$CaZrO_3$	20	Spray drying	650	90% CO_2	10	950	90% CO_2	0	30	0.61	0.47	Ultimate SP of CaO derived from spray drying method was enhanced by 1.24 times via doping with Zr-based metal oxide.	[55]
													23			
$Ca(NO_3)_2.4H_2O$ Calcium nitrate tetrahydrate	99.2	$Zr(NO_3)_4 \cdot 5H_2O$ zirconium nitrate pentahydrate	$CaZrO_3$	0.8	Revised sol-gel	600	50% CO_2	45	900	100% N_2	5	18	0.69	0.64	The modification with Zr-based metal oxide resulted in a 77.7% reduction in the SP deactivation.	[56]
													7.2			

$Ca(NO_3)_2$. H_2O Calcium nitrate hydrate	40	$ZrO(NO_3)_2$· xH_2O zirconium nitrate	$CaZrO_3$	60	Auto-combustion	650	20% CO_2 (in Ar)	20	900	80% CO_2 (in Ar)	20	12	0.31 0.26 / 16.1	The effectiveness of $CaZrO_3$ content on the durability of CaO particles	[57]
$Ca(CH_3COO)_2$· xH_2O Calcium acetate hydrate	80	$Zr(NO_3)_4$·xH_2O zirconium nitrate	$CaZrO_3$	20	Freeze drying	650	10% CO_2	15	900	15% CO_2	0	15	0.45 0.38 / 15.6	The final SP of CaO powder increased by 35.71 %	[58]
$Ca(NO_3)_2.4H_2O$ Calcium nitrate tetrahydrate	80	$ZrO(NO_3)_2.6H_2O$ zirconium oxynitrate hexahydrate	$CaZrO_3$	20	Solution combustion	675	20% CO_2	20	950	100% CO_2	20	50	0.53 0.29 / 45.3	The last-cycle SP of the modified sample is 2.823 times higher than the benchmark limestone.	[59]
$C_{22}H_{14}CaO_4$ calcium-naphthenate	23.8	$C_{32}H_{60}O_8Zr$ Zirconyl (IV) 2-ethyl hexanoate	$CaZrO_3$	76.2	Flame Spray Pyrolysis	700	99.5% CO_2	30	700	100% He	30	1200	0.11 0.11 / -	The modification led to stabilizing CaO adsorbents ultimately.	[60]
$Ca(C_2H_3O_2)_2·H_2O$ calcium acetate monohydrate	42	$ZrO(NO_3)_2$· xH_2O zirconium nitrate	$CaZrO_3$	58	Thermo-chemical	700	100% CO_2	30	750	100% Ar	30	15	0.19 0.135 / 28.94	The SP deactivation of unmodified CaO was decreased by 51.12% via modification.	[61]

2. Experimental

2.1. Raw materials:

In this research, $Ca(NO_3)_2.4H_2O$, calcium nitrate tetrahydrate from *Merck*, and $ZrO(NO_3)_2.H_2O$, zirconyl nitrate from *Sigma Alderich*, were used to develop $CaZrO_3$-containing CaO adsorbent. MWCNT additive from *VCN Materials Company*, with a diameter of 10-20 nm, a length of ~30 μm, a specific surface area of 200 m^2/g, a density of 2.1 g/cm^3, and purity of ≥ 98%, was employed as a flammable template.

2.2. Synthesis technique:

The specification of synthesized samples are reported in Table 2. All ZrO_2-stabilized CaO samples were prepared with the molar ratio of Ca/Zr: 15/1 and via the facile one-pot MWCNT-assistance thermochemical synthesis method. Firstly, the determined amounts of calcium nitrate, zirconium nitrate, and MWCNT powder were dissolved in deionized water based on the pertinent weight percentage. Then, the solution was uniformly heated and mixed for 60 min at 40℃. In the next step, the mixing temperature was raised to 100-110℃ to evaporate the water until gel formation. The formed gel was located in an oven under 150℃ to dry the gel and form a porous powder. The attained powder was calcined under airflow for 1.5 h at 850℃ in a furnace.

2.3. Characterization:

The specific surface area and pore size distribution of fresh adsorbents were determined employing BET/BJH analysis after degassing at 300℃ for 3 h in a vacuum and using N_2 adsorption/desorption at 77 K on BELSORP MINI II equipment. A Siemens 5 D500 X-ray diffractometer (Cu, K_α, λ= 0.15406 nm) was utilized to identify the formed crystalline phases in samples. XRD intensity results were collected over a 2θ range of 10-80°. To calculate the average CaO grain size of samples (D_{avg}), firstly, the grain size (D) of each crystalline CaO-based phases, including CaO (2θ= 32.32°, 37.47°, 53.93°), $Ca(OH)_2$ (2θ= 18.27°, 34.12°, 50.87°), and $CaCO_3$ (2θ= 25.22°, 27.28°, 29.53°, 32.87°), was estimated by Debye–Scherrer's equation [62-64]:

$$D = \frac{0.9 \times \lambda}{\beta \times \cos\theta} \quad (3)$$

θ and β are addressed to the half of the angular position and the total width at half of the peak intensity, respectively. Based on the average of the calculated Ds for each sample, D_{avg} was determined.

The morphology of fresh and used adsorbents was analyzed using FESEM analysis on FEI Quanta 200 microscope device, coupled with Oxford INCA sight X EDX test applying on SAMX detector to determine elemental dispersion.

The total Ca and Zr in the prepared samples were determined via ICP-OES analysis performed with a Varian Vista-PRO CCD Simultaneous ICP-OES equipment.

Multicyclic CO_2 uptake performance of developed adsorbents was analyzed with thermogravimetric analysis (TGA) via TA Instruments Discovery SDT 650 instrument. Practically at the realistic and severe post-combustion CO_2 capture processes, the fluidized-bed carbonator reactor operates at a short residence time due to the inlet high-velocity flue gas containing low CO_2 concentration. With entering combusting fuel to supply the required high temperature for CaO regeneration (≥ 900°C), calciner ambient constitutes the high CO_2 concentration (≥ 70% vol.). In this study, to acquire suitable outcomes and assess adsorbents' performance at the adjacent conditions to the practical applications, the prepared adsorbents have been analyzed under severe TGA conditions, which comprise:

(1) The CaO carbonation under the ambient containing 15 vol.% CO_2 balanced with 85 vol.% N_2, for 10 minutes at 650°C.

(2) The CaO regeneration (or $CaCO_3$ calcination) under the environment containing 100% CO_2 for 10 minutes at 650 °C.

The heating/cooling rate for all the steps was 50 °C/min. CO_2 sorption activity results were presented regarding CO_2 sorption capacity, cyclic durability, and total amount of captured CO_2, calculated as follows:

$$C_n = \frac{M_n - M_0}{M_0} \quad (4)$$

$$\text{Durability} = \frac{C_1 - C_{15}}{C_1} \times 100\% \quad (5)$$

$$T = \sum_{n=1}^{15} C_n \quad (6)$$

where C_n and M_n are addressed to the CO_2 capture capacity (g CO_2/ g adsorbent) and mass of adsorbent after the carbonation of the n^{th} cycle, respectively. Accordingly, C_1 and C_{15} are

related to the CO_2 capture capacity of the adsorbent at the 1^{st} and 15^{th} cycles. M_0 is the primary mass of adsorbent before starting the first cycle. Moreover, T is the cyclic durability (the total amount of captured CO_2 (g CO_2/ g adsorbent).

Table 2: Specification of developed MWCNT-templated ZrO_2-stabilized CaO samples.

Sorbent	Elemental composition (At. %)[a]		Ca/Zr molar ratio		Phase compositions (wt.%)		Average CaO grain size (nm)	Textural parameters		
	Ca	Zr	Nominal	Actual [a]	CaO	$CaZrO_3$		S_{BET}[b] (m^2/g)	S_{Lang}[b] (m^2/g)	V_p[c] (mm^3/g)
CaZr	47.82	3.2	15/1	14.94/1	81.5	18.5	42.6	1.75	1.49	25.4
CaZr-CNT2.5	45.08	2.98	15/1	15.13/1	81.5	18.5	38.1	2.53	2.75	26.01
CaZr-CNT5	37.86	2.53	15/1	14.96/1	81.5	18.5	27.7	6.03	7.25	56.4
CaZr-CNT10	35.42	2.35	15/1	15.07/1	81.5	18.5	28.1	4.99	5.64	61.25

a. Obtained by ICP analysis.

b. S_{BET} and S_{Lang}: specific surface area.

c. V_p: BJH pore volume.

3. Results and discussion:

To evaluate the influence of MWCNT on textural and structural features and sorption activity of $CaO/CaZrO_3$ adsorbent, various contents of MWCNT, 2.5, 5, and 10 wt.%, are incorporated into $CaZrO_3$-supported CaO adsorbent.

3.1. Characterization

The structural and textural characteristics of CaZr, CaZr-CNT2.5, CaZr-CNT5, and CaZr-CNT10 are presented in Table 2. The stoichiometric $CaO/CaZrO_3$ (wt.%) of 81.5/18.5 acquires for all prepared samples. The Ca/Zr molar ratios derived from ICP analysis are reported in Table 2. The Ca/Zr molar ratios of 14.94, 15.13, 14.96, and 15.07 indicate differences ratios (%) of 0.4, 0.86, 0.26, and 0.46%, with a Ca/Zr molar ratio of 15/1, for CaZr, CaZr-CNT2.5, CaZr-CNT5, and CaZr-CNT10, respectively, which corroborates the initial employed Ca/Zr molar ratio of 15/1 during samples' preparation. There is symmetric conformity between the calculated CaO grain size and the measured surface area and pore volume. Fig. 1 shows that the measured pore volumes and surface areas are inversely proportional to the calculated CaO grain sizes. The reduction in the CaO grain size and increase in the surface area by doping $CaO\text{-}CaZrO_3$ adsorbent with MWCNT additive reveal the effectiveness of MWCNT combustion on its structural and textural features. Merging 5 and 10 wt.% of MWCNT with CaZr adsorbent dramatically increases CaZr surface area 2.44 and 1.85 times, respectively. This promotion in the textural characterizations of CaZr after doping with ≥ 5 wt.% MWCNT facilitates the diffusion of $CaZrO_3$ species into the interior zones to mitigate the grain agglomeration phenomenon. A reduction in the accessible surface area of CaZr-CNT10 than that of CaZr-CNT5 arises from the significant increase in the volume of macropores in CaZr-CNT10 compared to CaZr-CNT5. With the increase of the merged MWCNT content from 5 wt.% to 10 wt.% and embedding more MWCNTs into CaO structures, not only more high-volume pores were formed through the combustion of embedded MWCNT particles and corresponding their vacancy, but also more gas volume was released that resulted in the formation of macropores with higher volumes in CaO texture.

XRD patterns of CaZr, CaZr-CNT2.5, CaZr-CNT5, and CaZr-CNT10 adsorbents are presented in Fig. 2. Ca-based phases, including CaO, $Ca(OH)_2$, and $CaCO_3$, are the principal components with high-intensity peaks for CaZr, CaZr-CNT2.5, CaZr-CNT5, and CaZr-CNT10. The XRD patterns exhibit the development of $CaZrO_3$ in ZrO_2-containing adsorbents.

$CaZrO_3$ species are developed via a direct solid-solid reaction between CaO and ZrO_2, in which Ca^{+2} diffuses into the ZrO_2 interface and lattice over synthesis steps. The applied synthesis technique evolves the temperature of ≥ 1000°C to form $CaZrO_3$, constructively [38, 65-67]. The main reason for the formation of the $CaCO_3$ phase in the cases of CaZr-CNT5 and CaZr-CNT10 is related to the adsorption of CO_2 on the reaction interface of CaO nanoparticles during the cooling stage of post calcination of samples in the furnace. The higher intensity of $CaCO_3$ peaks in the cases of CaZr-CNT5 and CaZr-CNT10 stems from their higher surface area and pores [68]. The physically adsorbed CO_2 and H_2O in the forms of $Ca(OH)_2$ and $CaCO_3$ are desorbed in the heating stage of pre-carbonation in the TGA test.

Fig. 3a shows the N_2 adsorption/desorption isotherms of CaZr, CaZr-CNT2.5, CaZr-CNT5, and CaZr-CNT10 in P/P_0 ranged between 0 and 1. Due to substantial symmetry in shape, N_2 adsorption/desorption isotherms of all samples are classified as type II mode, which standardly demonstrates mesoporous texture [69, 70]. These adsorbents possess the hysteresis loop type of H3, determined over hair-like high-pressure condensation of N_2 molecules in mesopores ($0.8 \leq P/P_0 \leq 1$ stage). This hysteresis loop type reveals the aggregation of plate-like CaO particles, leading to the appearance of slit-shaped pores [71, 72]. The slow diffusion of inlet gas to acquire equilibrium adsorption leads to the explicit hysteresis for these isotherms at $0 \leq P/P_0 \leq 0.1$ within the range of each adsorption stage [72]. These isotherms indicate the macro-porous structure.

BJH pore size distributions of CaZr, CaZr-CNT2.5, CaZr-CNT5, and CaZr-CNT10 at pore diameters ranging from 1-10 and 10-100 nm are depicted in Fig. 3b. All samples illustrate the wide pore volume distribution. By integrating CaZr with ≥ 5 wt.% MWCNT, the formation of high-diameter pores (pore diameter ≥ 10 nm) is dramatically increased (see Fig. 6d), which can be well attributed to more inclusive dispersion of embedded MWCNT between CaO nanoparticles and more importantly, emission of large volumes of combustion gases. As reported in Table 2, the pore volume of CaZr increases from 25.4 mm^3/g to 26.01, 56.4, and 61.25 mm^3/g, with improvement rates (%) of ~2.4, ~122, and ~141%, after merging with 2.5, 5, and 10 wt.% MWCNT, respectively. Having being modified with 2.5 and 5 wt.% MWCNT, higher mesopores are formed, and so the higher value of BET surface area for CaZr-CNT5 (6.03 m^2/g) compared to CaZr-CNT2.5 (2.53 m^2/g), and CaZr-CNT10 (4.99 m^2/g) can be ascribed to its higher volume of mesopores (see Fig. 6c). On the other hand, the most multitude of macropores is developed in the case of CaZr-CNT10. Although free surface area decreased by increasing the content of added MWCNT from 5 wt.% to 10 wt.%, BJH pore volume

improved ~8%. The higher volume of macropores in the case of CaZr-CNT10 is the main reason for its higher BJH pore volume and lower surface area among MWCNT-templated ZrO_2-containing CaO adsorbents. As a significant finding, incorporating ≥ 5 wt.% MWCNT into CaZr adsorbents leads to highly porous structures associated with significantly improved surface area and pore volume.

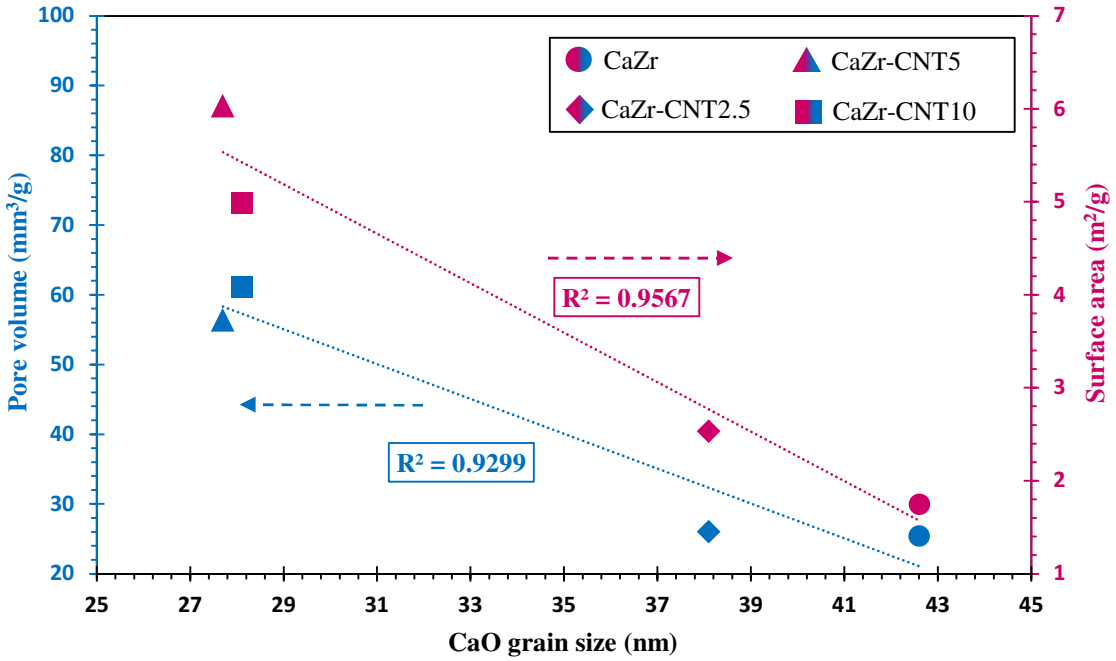

Fig. 1: Pore volume and surface area of CaZr, CaZr-CNT2.5, CaZr-CNT5, and CaZr-CNT10 adsorbents versus CaO grain size.

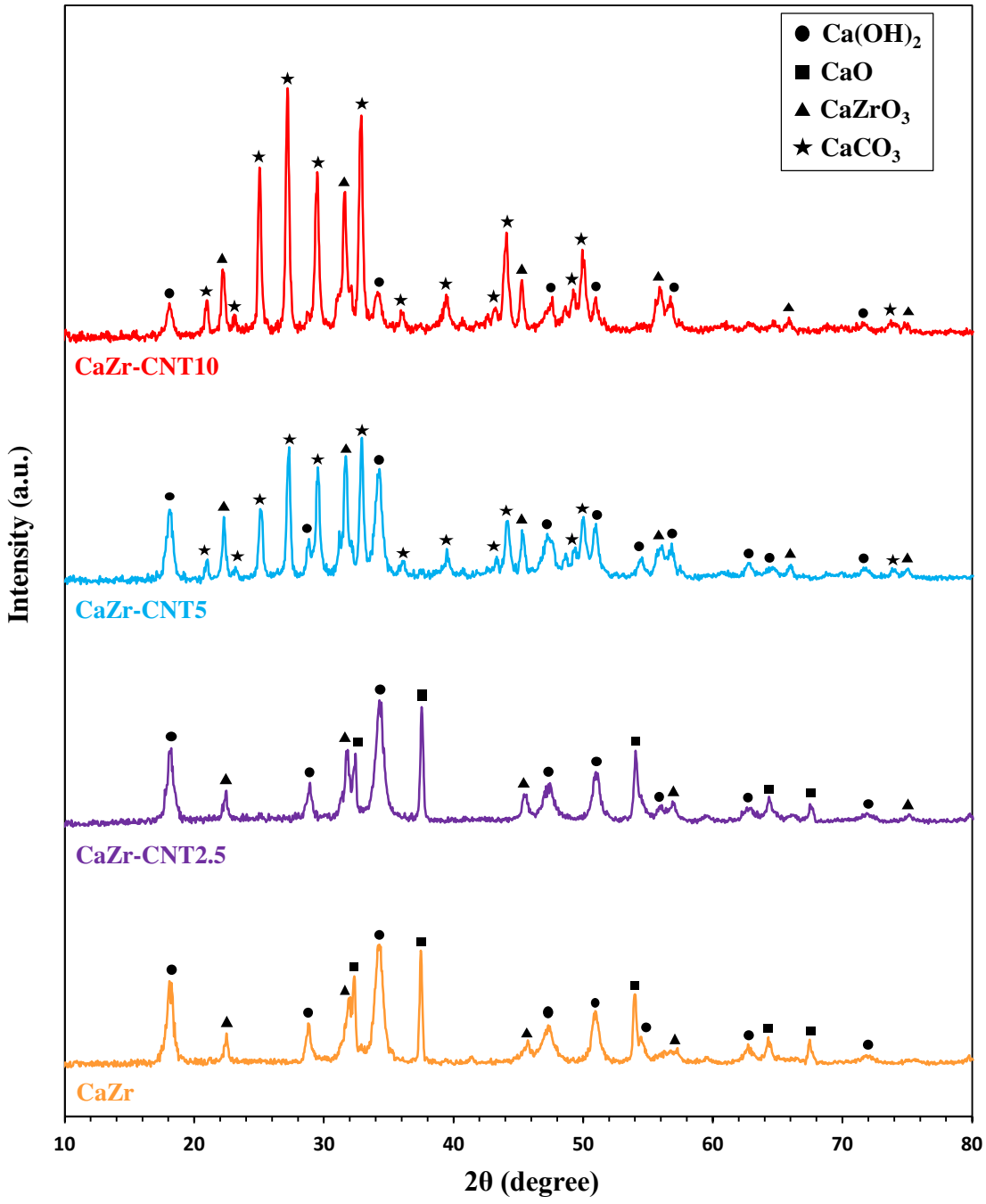

Fig. 2: XRD patterns of the developed CaO-derived adsorbents.

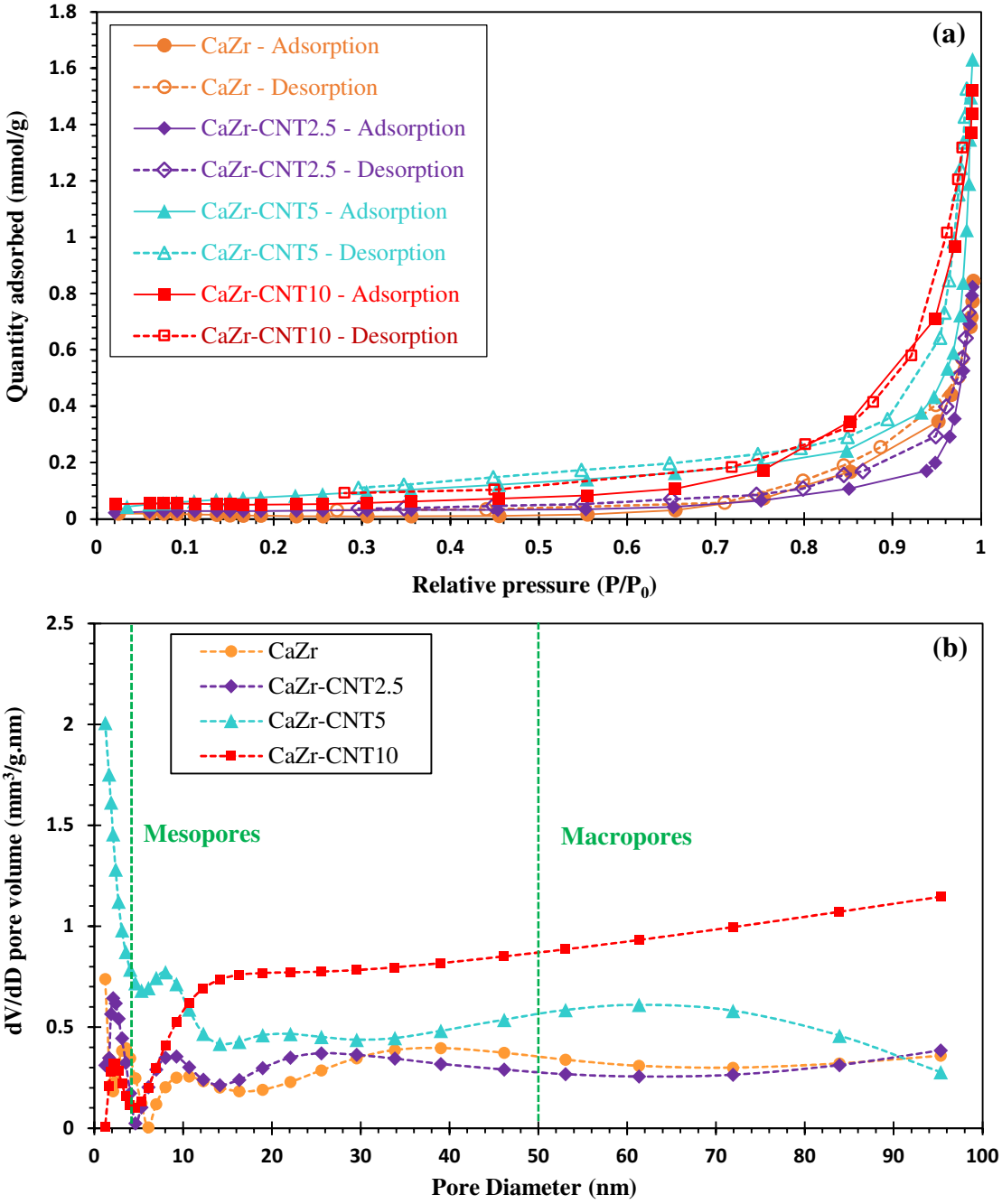

Fig. 3: (a) N_2 adsorption/ desorption isotherm, (b) pore size distribution curves for CaZr, CaZr-CNT2.5, CaZr-CNT5, and CaZr-CNT10 adsorbents.

Fig. 4 shows FESEM micrographs and EDX dot-mappings of CaZr, CaZr-CNT2.5, CaZr-CNT5, and CaZr-CNT10. With MWCNTs being added, more porosity emerges in the compact morphology of CaZr. Even though the elemental EDX exhibits the attendance of Zr on the surface of CaZr, the grade-shape morphology of CaZr can be attributed to non-uniform distribution and insufficient attendance of $CaZrO_3$ among the surface-resident CaO particles, as presented in EDX dot-mapping of CaZr. Comparing morphological characteristics of MWCNT-templated CaZr adsorbents with CaZr reveals the formation of more porous

structures associated with smaller surface-located CaO grain sizes and more presence of $CaZrO_3$ among surface-resident CaO particles. In addition to developing a more fluffy-like texture, micro-, and macropores, MWCNTs affect the distribution of $CaZrO_3$ among CaO grains. The elemental EDX spectrum of four samples demonstrates the presence of Ca, Zr, C, and O elements related to developed CaO, $Ca(OH)_2$, $CaCO_3$, and $CaZrO_3$ phases. Comparing FESEM pictures of CaZr-CNT2.5, CaZr-CNT5, and CaZr-CNT10 represent the higher porous zones, and less-diameter CaO grains appear in the CaO textures of CaZr-CNT10. EDX dot-mapping images are presented to evaluate the influence of embedded MWCNT on the $CaZrO_3$ distribution between CaO nanoparticles. Even though the $CaZrO_3$ grains were heterogeneously dispersed on the surface of CaZr-CNT2.5 and CaZr-CNT5, the EDX image of CaZr-CNT10 indicates the homogeneous dispersal of $CaZrO_3$ on the sorbent's morphology. The effect of embedded MWCNT on the distribution of $CaZrO_3$ can be the secondary reason for the more porous structure of CaZr-CNT10 among developed samples. Conformed with previously reported textural characteristics, among developed samples, as it is apparent in the FESEM images, CaZr-CNT10 possesses a higher volume of pores.

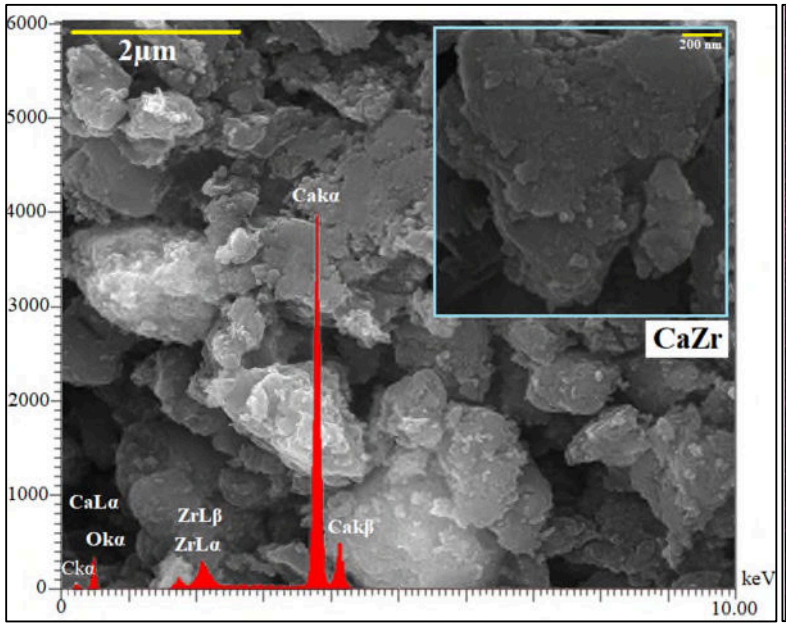
2µm
200 nm
CaZr
Caκα
CaLα
Oκα
Cκα
ZrLβ
ZrLα
Caκβ
keV
0
10.00
6000
5000
4000
3000
2000
1000
0

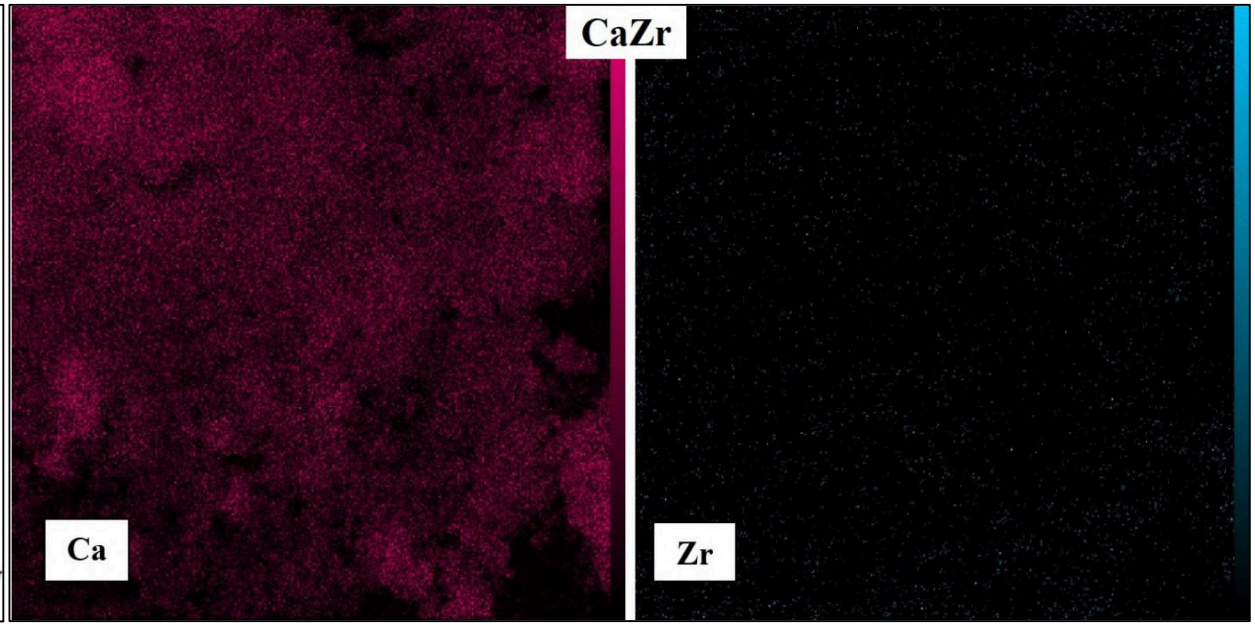
CaZr
Ca
Zr

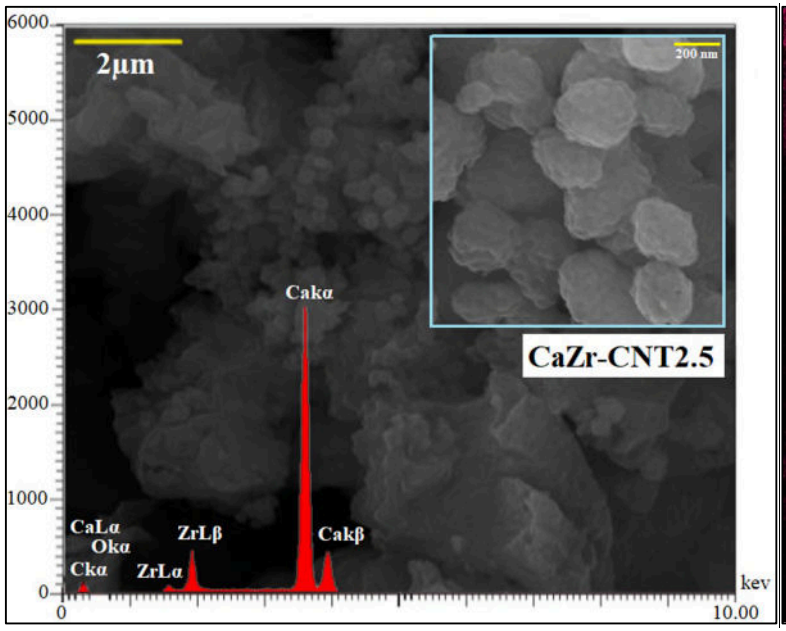
2µm
200 nm
CaZr-CNT2.5
Caκα
CaLα
Oκα
Cκα
ZrLβ
ZrLα
Caκβ
kev
0
10.00
6000
5000
4000
3000
2000
1000
0

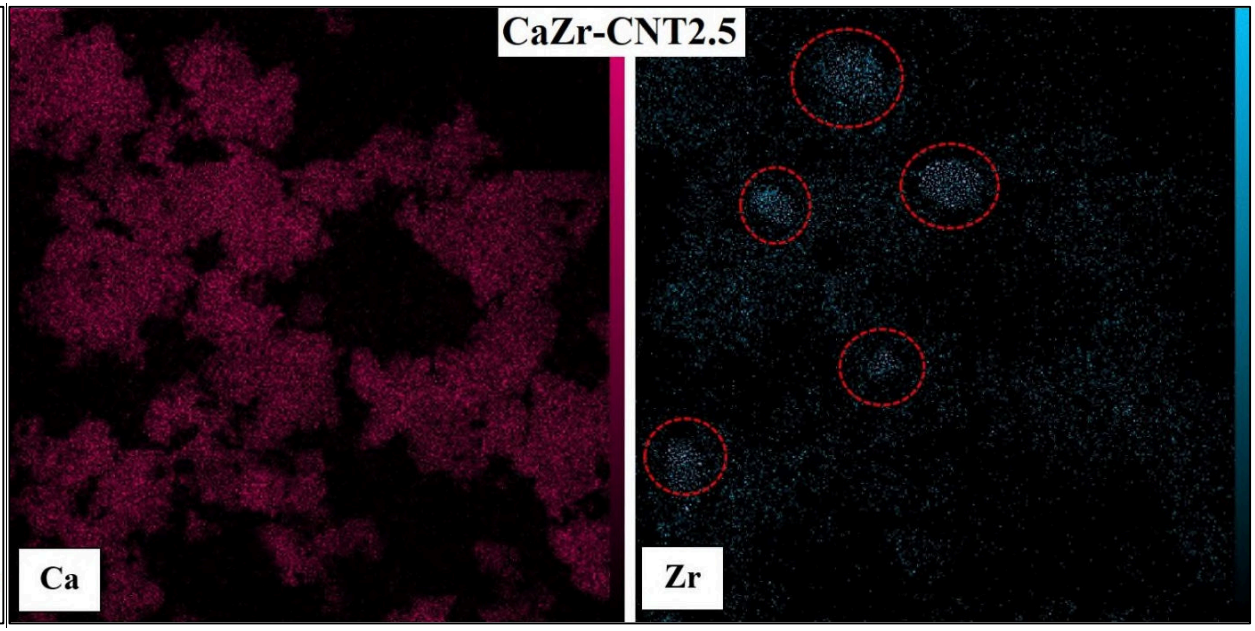
CaZr-CNT2.5
Ca
Zr

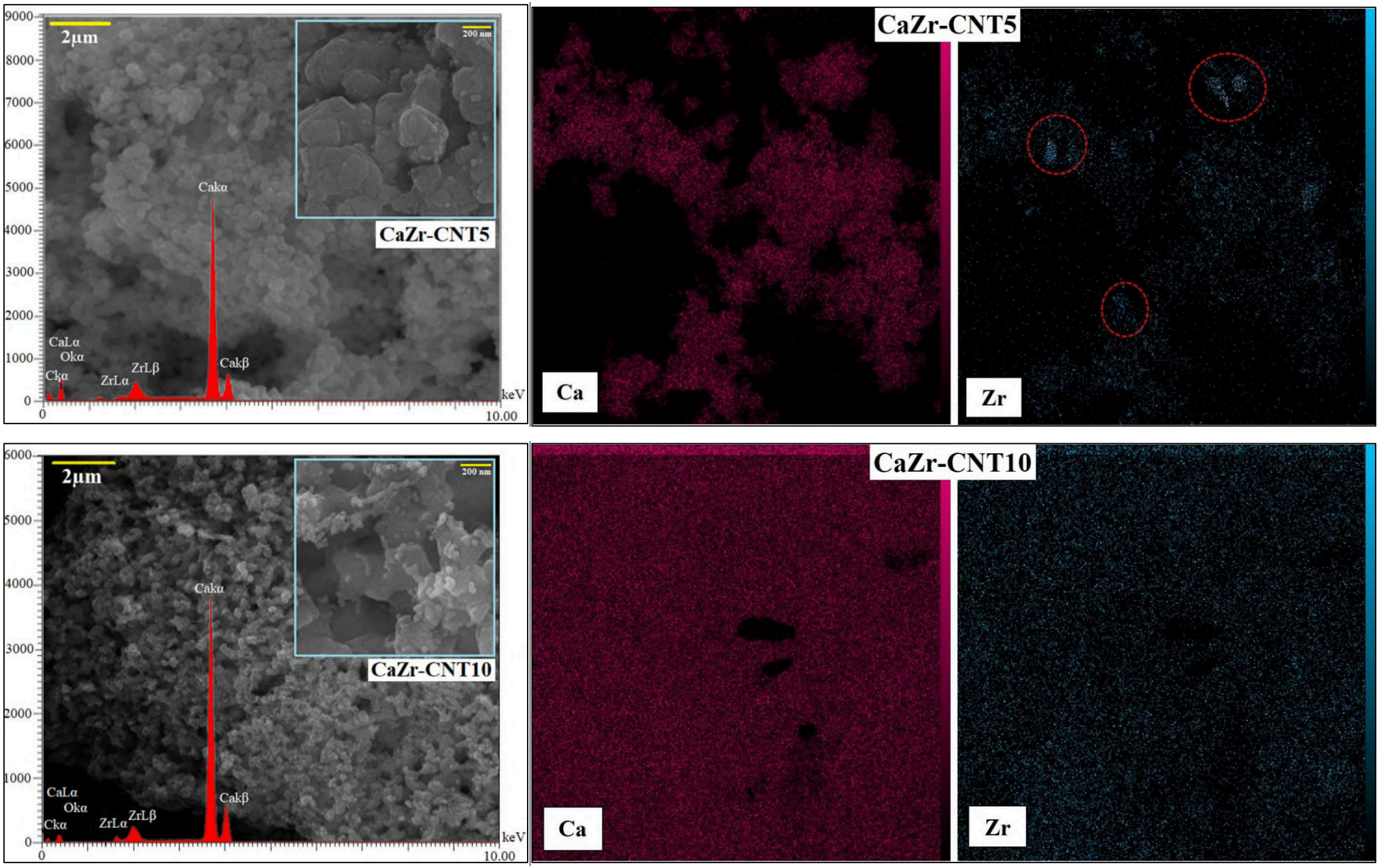

Fig. 4: FESEM micrographs and EDX dot-mappings of developed adsorbents.

3.2. Sorption performance

To assess the influence of adding disparate mass percentages of MWCNT on the sorption activity of CaZr adsorbent, CO_2 capture capacity of CaZr, CaZr-CNT2.5, CaZr-CNT5, and CaZr-CNT10 adsorbents during fifteen multiple carbonation/calcination cycles under severe CaL conditions is measured and presented in Fig. 5. MWCNT-templated $CaO/CaZrO_3$ adsorbents exhibit better sorption activity than CaZr samples. Incorporating MWCNT into CaZr adsorbent enhances CO_2 capture capacity, and therefore, CaZr-CNT2.5, CaZr-CNT5, and CaZr-CNT10 demonstrate the highly enhanced cyclic durability compared to CaZr. Although the highest initial sorption capacity among the MWCNT-templated $CaO/CaZrO_3$ adsorbents is related to CaZr-CNT5, CaZr-CNT10 shows superior sorption capacity. The higher initial sorption capacity of CaZr-CNT5 can be attributed to its highest surface area among prepared samples (see Table 2). The detailed sorption activity of MWCNT-incorporated $CaO/CaZrO_3$ adsorbents and CaZr is reported in Table 3. The total amount of captured CO_2 for CaZr over fifteen multiple cycles, 0.6 g CO_2/g adsorbent, reaches up to 0.93, 1.47, and 1.7 for CaZr-CNT2.5, CaZr-CNT5, and CaZr-CNT10, respectively, which indicates 55, 145, and 183.3% improvement rate, respectively. Moreover, CaZr-CNT2.5, CaZr-CNT5, and CaZr-CNT10 maintain 32.36, 42.84, and 61.12% of their initial sorption capacity, whereas CaZr shows the sorption activation of 29.5% over fifteen multiple cycles. The principal reason for the superior cyclic durability of CaZr-CNT 10 is the more efficient and broader dispersion of $CaZrO_3$ between CaO nanoparticles. In addition to outstanding improved morphological and constructional characteristics (see Figs. 3 and 4 and Table 2), the higher sorption capacity of CaZr-CNT5 and CaZr-CNT10 than CaZr demonstrate the effectiveness of MWCNT as a promoter template in improving the sorption activity of CaZr adsorbents. Among these samples, CaZr-CNT10 indicates superior cyclic activity and possesses more porosity (larger pore volume and pore size).

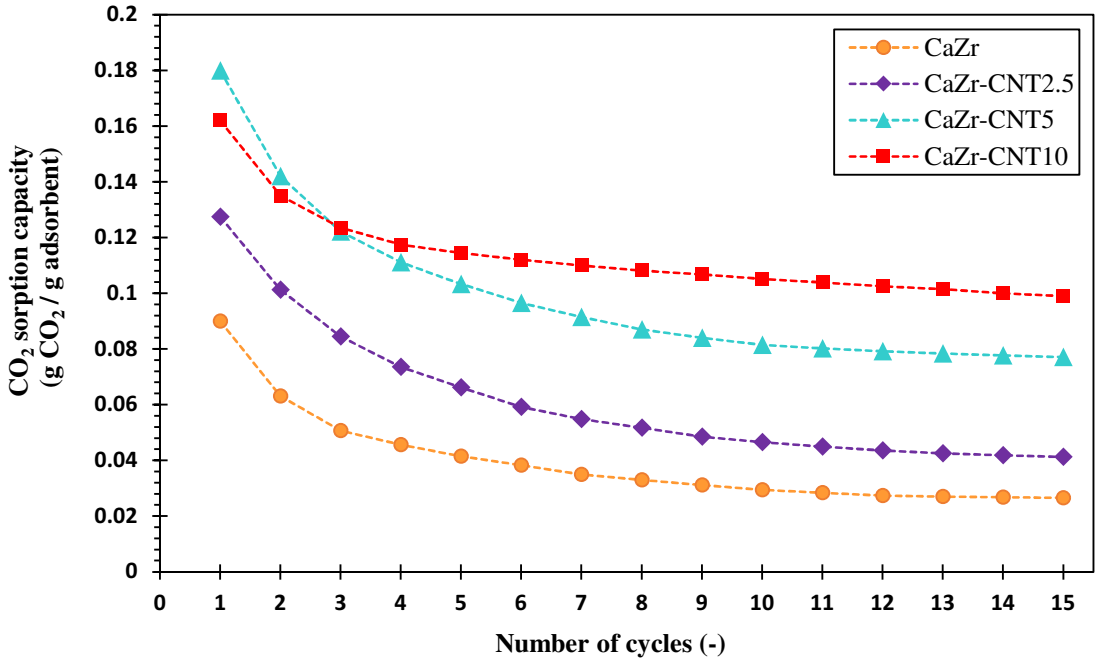

Fig. 5: CO_2 sorption capacity of CaZr, CaZr-CNT2.5, CaZr-CNT5, and CaZr-CNT10 adsorbents during 15 multiple carbonation/calcination cycles.

Table 3: CO_2 sorption activity of developed adsorbents.

Adsorbent	CO_2 sorption capacity (g CO_2/g adsorbent)		Maximum CO_2 sorption rate cg CO_2/(g adsorbent.min)		The total amount of captured CO_2 over 15 cycles (g CO_2/g adsorbent)	Cyclic durability (%)
	1st cycle	15th cycle	1st cycle	15th cycle		
CaZr	0.09	0.03	4.11	1.5	0.6	29.5
CaZr-CNT2.5	0.13	0.04	6.78	2.37	0.93	32.36
CaZr-CNT5	0.18	0.08	10.31	3.68	1.47	42.84
CaZr-CNT10	0.16	0.1	11.47	12.88	1.7	61.12

CO_2 capture capacity and rate of CaZr, CaZr-CNT2.5, CaZr-CNT5, and CaZr-CNT10 adsorbents over carbonation time at 1st and 15th cycle under severe CaL conditions are shown in Fig. 6a and b, respectively. The CO_2 sorption rate swiftly rises during the kinetically-controlled carbonation stage, which lasts 0.5 min, and culminates in the maximum CO_2 sorption rate at the terminal of the fast carbonation stage. With the onset of the diffusion-controlled stage, the sorption rate of all samples quickly drops due to the saturation of accessible CaO sites by growing the $CaCO_3$ product layer. The CO_2 sorption capacity of all samples versus time ranging from 0.5-10 min increases slowly in the CO_2 sorption capacity plot due to the transmission of the fast stage to the slow carbonation stage. Considering Table

3, CaZr-CNT5 exhibits the highest sorption capacity in 1st cycle and the highest maximum sorption rate (11.47 cg/g.min). However, at the 15th cycle, the highly superior CO_2 sorption rate and capacity are presented by CaZr-CNT10. This increase in sorption capacity of CaZr-CNT10 confirms its excellent porosity than CaZr, CaZr-CNT2.5, and CaZr-CNT5 even after 15 multicycles. Comparing both plots indicates the sintering effect on sorption activity of all samples, which decreases sorption capacity at both carbonation stages.

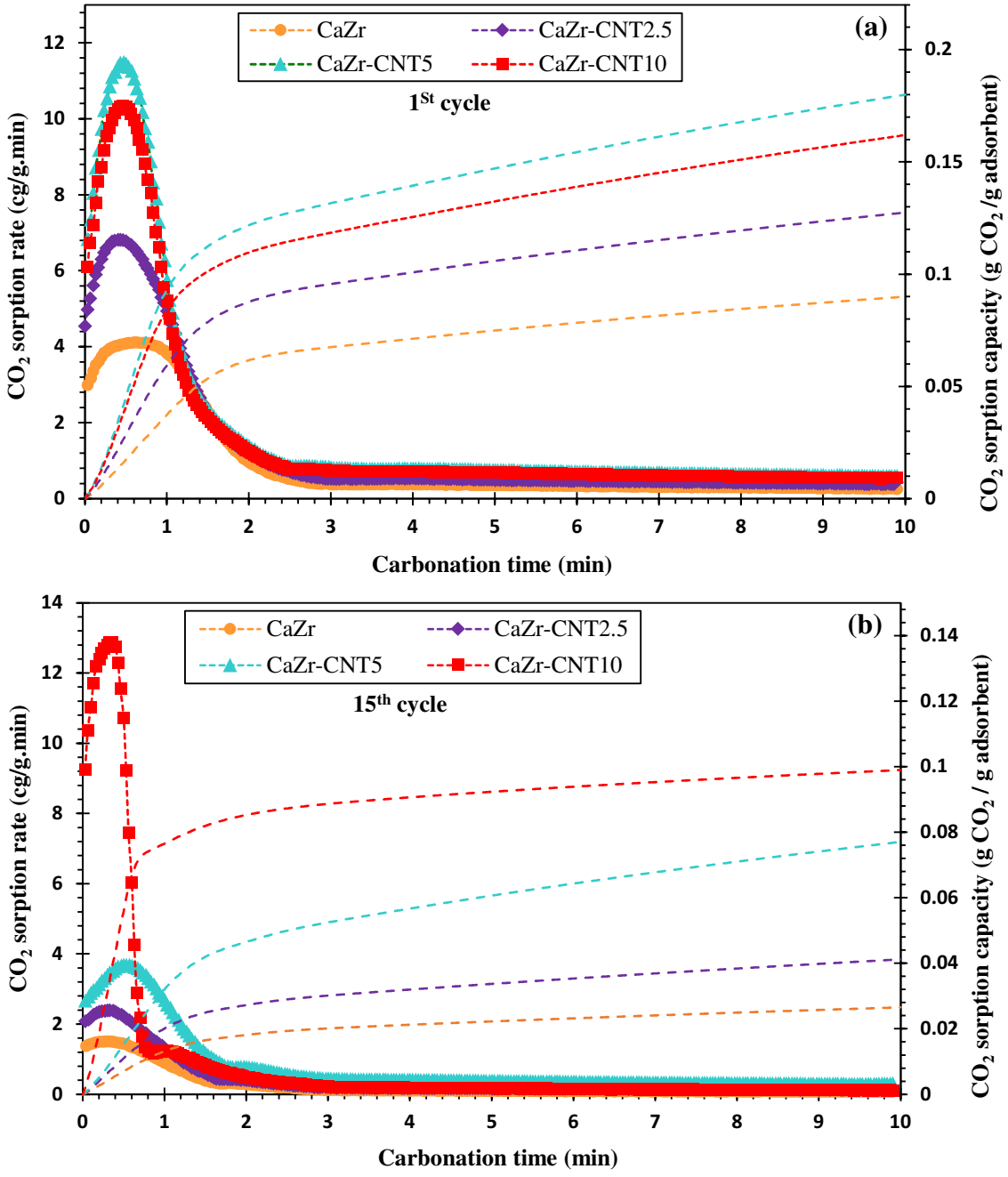

Fig. 6: CO_2 sorption capacity and rate of CaZr, CaZr-CNT2.5, CaZr-CNT5, and CaZr-CNT10 adsorbents versus carbonation time at 1st and 15th cycle.

To recognize sintering-caused morphological transformations over 15 multiple carbonation/calcination cycles, the FESEM micrographs of used MWCNT-templated $CaZrO_3$-containing CaO adsorbents are illustrated in Fig. 7. Representative pictures demonstrate the sintering phenomena in all samples' surfaces. Less porosity, more surface agglomeration, and more surface-resident particle sizes are observed for all cycled adsorbents, indicating the sintering phenomenon. Among all samples, CaZr-CNT10 maintained more active CaO cites after the CaL process. The superior CO_2 capture activity of CaZr-CNT10 (see Table 3) is conformed with its more porous texture, more non-sintered zones, and more diffusible pores after 15 multiple cycles compared with used CaZr, CaZr-CNT2.5, and CaZr-CNT5.

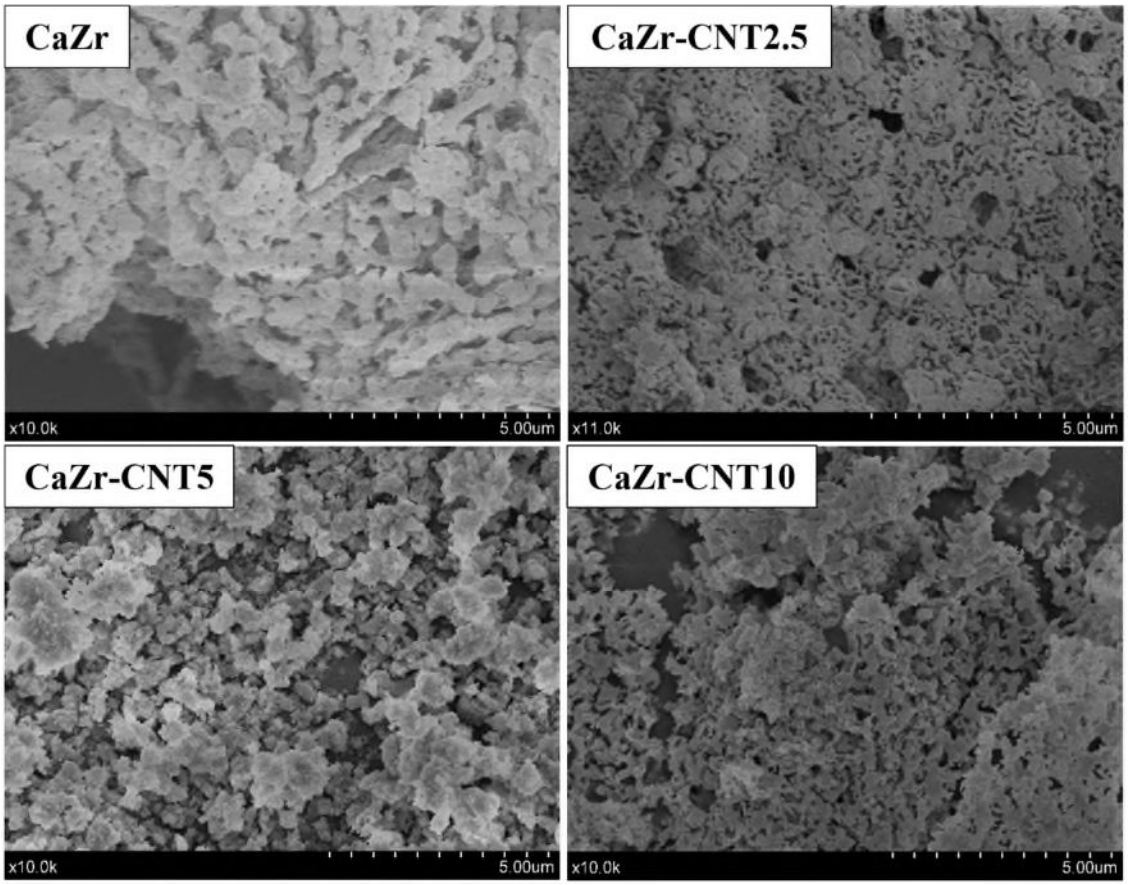

Fig. 7: FESEM images of developed samples after passing 15 cycles.

Fig. 8a manifests the effectiveness of the BET surface area of uncycled samples on their CO_2 uptake potential. The initial CO_2 sorption capacity of developed samples is linearly symmetrical to their BET surface area, in which CaZr and CaZr-CNT5 with the lowest and highest surface area (1.75 and 6.03 mm^2/g), respectively, possess the least and most CO_2 sorption capacity at 1st cycle (0.09, and 0.18 g CO_2/g adsorbent, respectively). It is worth stating that the adsorbent with a higher BET surface area possesses significantly more accessible CaO sites to adsorb CO_2 molecules during the kinetically-controlled carbonation stage.

Consequently, most initial CO_2 sorption capacity of CaZr-CNT5 among all samples stems from its highest surface area.

The total amount of captured CO_2 over 15 multicycles under realistic CaL conditions for CaZr, CaZr-CNT2.5, CaZr-CNT5, and CaZr-CNT10 versus BJH pore volume is exhibited in Fig. 8b. BJH pore volume has an efficient role in the total amount of captured CO_2, which linearly enhances with increasing pore volume. Pointing to the lower pore volume of CaZr, all MWCNT-templated $CaO/CaZrO_3$ adsorbents that possess higher pore volume adsorb more amount of CO_2 during the CaL process, in order of CaZr-CNT10 (1.7) > CaZr-CNT5 (1.47) > CaZr-CNT2.5 (0.93) > CaZr (0.6). It can be noted as the fundamental outcome that increasing the amount of incorporated MWCNT in CaZr adsorbents leads to enhancing the amount of captured CO_2 over fifteen CaL cycles, which stems from raising pore volume.

Fig. 8c presents the improvement rate (%) in the essential textural and multicyclic parameters, including BJH pore volume, BET surface area, cyclic durability, and the total amount of captured CO_2 versus the amount of incorporated MWCNT into CaZr to assess the influence of MWCNT. The improvement rates (%) of all parameters increase with increasing the amount of MWCNT. For instance, doping with 10 wt.% MWCNT, BJH pore volume, BET surface area, cyclic durability, and the total amount of captured CO_2 of CaZr enhance by 141.1, 185.1, 107, 183.3%, respectively. These conspicuous enhancements (Fig. 8c) of CaZr characterizations disclose the effectiveness of incorporating MWCNT into CaO-based adsorbents to acquire highly improved structural properties and CO_2 sorption activity.

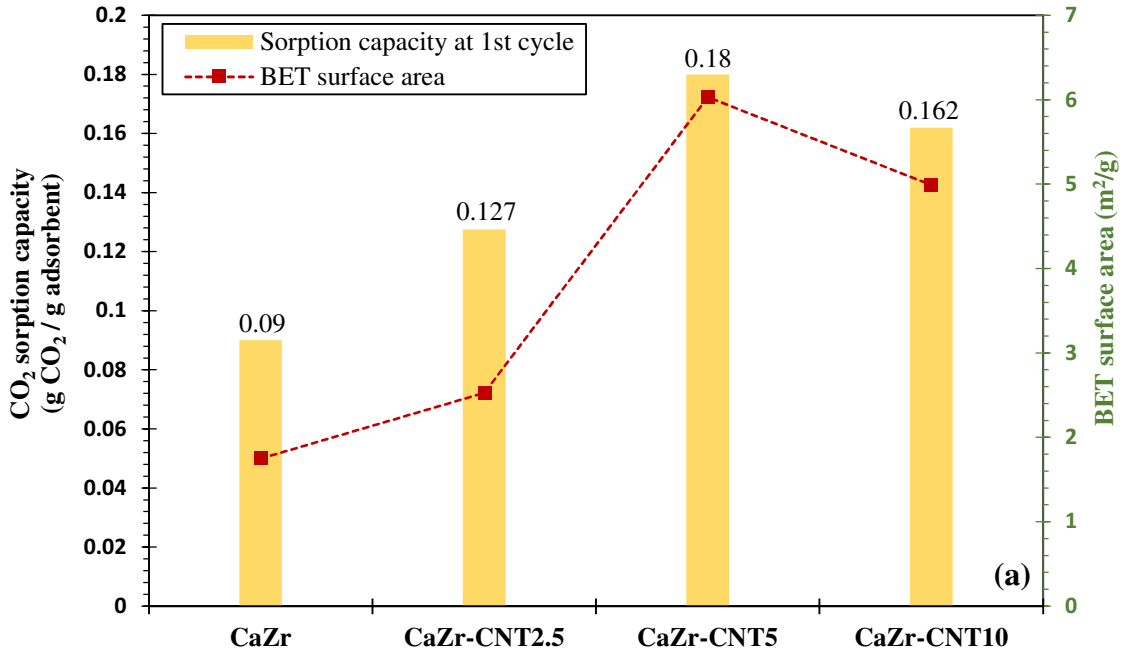
Sorption capacity at 1st cycle
BET surface area
0.09
0.127
0.18
0.162
(a)
CaZr
CaZr-CNT2.5
CaZr-CNT5
CaZr-CNT10
CO2 sorption capacity (g CO2 / g adsorbent)
BET surface area (m2/g)

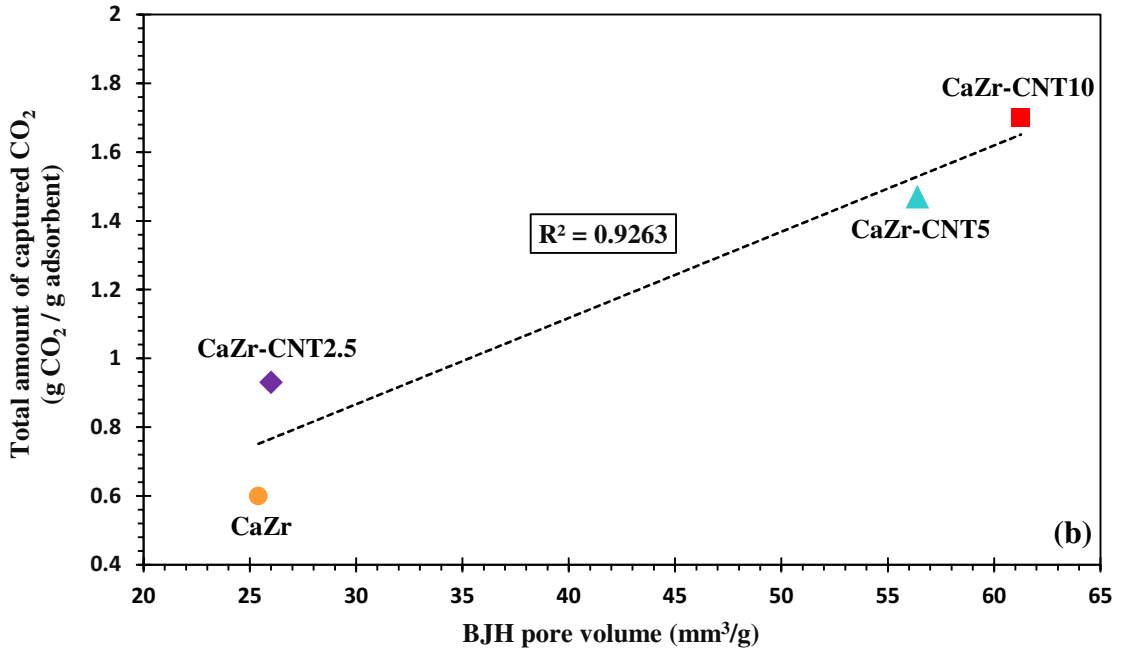
R² = 0.9263
CaZr-CNT10
CaZr-CNT5
CaZr-CNT2.5
CaZr
(b)
Total amount of captured CO2 (g CO2 / g adsorbent)
BJH pore volume (mm3/g)

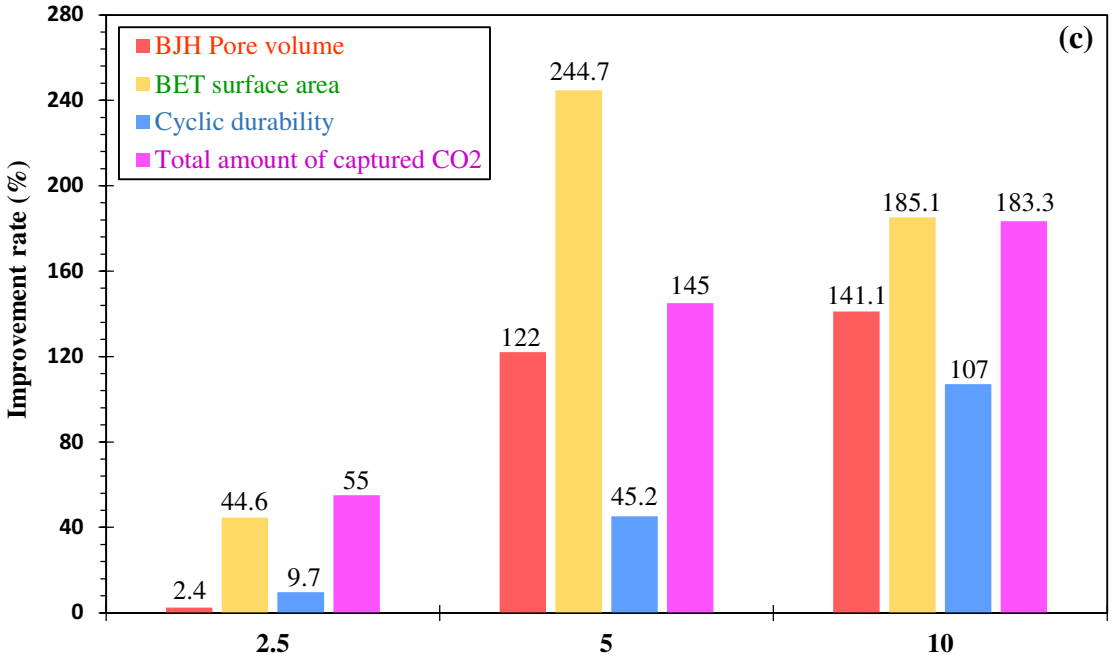

Fig. 8: (a) CO_2 sorption capacity of CaZr, CaZr-CNT2.5, CaZr-CNT5, and CaZr-CNT10 adsorbents at 1st multiple carbonation/calcination cycles under realistic CaL conditions versus BET surface area, (b) Total amount of captured CO_2 by CaZr, CaZr-CNT2.5, CaZr-CNT5, and CaZr-CNT10 adsorbents over fifteen multiple carbonation/calcination cycles under the realistic CaL conditions versus BJH pore volume, and (c) Improvement rate (%) of BJH pore volume, BET surface area, cyclic durability, and the total amount of captured CO_2 in CaZr by doping with 2.5, 5, and 10 wt.% of MWCNT.

4. Conclusion

Herein, we aim to develop a highly efficient CaO-based adsorbent via a facile one-pot MWCNT-assistance preparation method for the CO_2 capture process. Firstly, Zr-containing CaO-based adsorbents containing 18.5 wt.% $CaZrO_3$ were doped with 2.5, 5, and 10 wt.% MWCNT. The influence of MWCNT on textural properties, morphology, and CO_2 capture activity of Zr-containing CaO adsorbents was characterized by XRD, BET, N_2 adsorption/desorption, BJH, SEM micrographs, EDX elemental and dot-mapping, and TGA. Based on the characterizations' results, incorporating MWCNT into CaO configuration improves the structural, morphological, and textural properties of CaZr adsorbents. By employing 5 and 10 wt.% of MWCNT, the pore volume of CaZr increases by 122 and 141.1%, associated with 244.4 and 185.1% increment in surface area, respectively. Additionally, the addition of 5 and 10 wt.% of MWCNT during the preparation of Zr-promoted CaO adsorbents led to 34.97 and 34.04 % reduction in CaO grain size, indicating the improvement in CaO texture. Conformed with representative SEM images, the appearance of meso- and macropores in the inner zones of prepared adsorbents boosts the porosity of CaZr-based adsorbents. In addition to a structural improvement, there are significant enhancements in cyclic durability and CO_2 capture capacity of Zr-containing CaO adsorbents by using an MWCNT additive.

According to TGA test outcomes, in addition to 45.2 and 107 % enhancement in CO_2 capture durability, 145 and 183.3% increment in the total amount of captured CO_2 over 15 multiple carbonation/calcination cycles are acquired with the usage of 5 and 10 wt.% of MWCNT during developing Zr-containing CaO adsorbents. The reported improvement rate in CO_2 capture features of modified adsorbents is potentially related to the improved textural and morphological properties, specially CaO grain size. Furthermore, it can be attributed to the more homogeneous distribution of $CaZrO_3$ species in MWCNT-templated adsorbents facilitated by decreasing CaO grain sizes. The aforementioned remarkable increment ratio in textural and multicyclic features of CaZr demonstrates the highly determinative role of MWCNT in improving CaO adsorbents.

Author contribution:

Seyed Borhan Mousavi: Investigation, Conceptualization, Methodology, Formal analysis, Writing original draft. **Mohammad Heidari**: Investigation, Conceptualization, Methodology, Formal analysis, Project Administration, Writing original draft. **Farhad Rahmani**: Supervision, Project administration, Visualization, Conceptualization, Review & Editing. **Rojiar Akbari Sene:** Investigation, Review & Editing. **Peter Clough**: Review & Editing. **Serap Ozmen:** Investigation.

References:

[1] M. Ebratkhahan, S. Naghash Hamed, M. Zarei, A. Jafarizad, M. Rostamizadeh, Removal of neutral red dye via electro-fenton process: a response surface methodology modeling, Electrocatalysis 12(5) (2021) 579-594.
[2] M. Tahmasebpoor, S. Hosseini Nami, M. Khatamian, L. Sanaei, Arsenate removal from contaminated water using Fe2O3-clinoptilolite powder and granule, Environmental Technology 43(1) (2022) 116-130.
[3] M. Ashrafivala, S.B. Mousavi, S. Zeinali Heris, M. Heidari, M. Mohammadpourfard, H. Aslani, Investigation of H2O2/UV advanced oxidation process on the removal rate of coliforms from the industrial effluent: A pilot-scale study, International Journal of Hydrogen Energy 47(78) (2022) 33530-33540.
[4] O. Mynko, I. Amghizar, D.J. Brown, L. Chen, G.B. Marin, R.F. de Alvarenga, D.C. Uslu, J. Dewulf, K.M. Van Geem, Reducing CO2 emissions of existing ethylene plants: Evaluation of different revamp strategies to reduce global CO2 emission by 100 million tonnes, Journal of Cleaner Production 362 (2022) 132127.
[5] J. Rogelj, D. Huppmann, V. Krey, K. Riahi, L. Clarke, M. Gidden, Z. Nicholls, M. Meinshausen, A new scenario logic for the Paris Agreement long-term temperature goal, Nature 573(7774) (2019) 357-363.
[6] Y. Wang, X. Liu, H. Zhang, Y. Liu, P. Cui, Z. Zhu, Y. Ma, J. Gao, Comprehensive 3E analysis and multi-objective optimization of a novel process for CO2 capture and separation process from syngas, Journal of Cleaner Production 274 (2020) 122871.
[7] M.D.G. de Luna, A.S. Sioson, A.E.S. Choi, R.R.M. Abarca, Y.-H. Huang, M.-C. Lu, Operating pH influences homogeneous calcium carbonate granulation in the frame of CO2 capture, Journal of Cleaner Production 272 (2020) 122325.
[8] J. Ma, D. Mei, W. Peng, X. Tian, D. Ren, H. Zhao, On the high performance of a core-shell structured CaO-CuO/MgO@ Al2O3 material in calcium looping integrated with chemical looping combustion (CaL-CLC), Chemical Engineering Journal 368 (2019) 504-512.
[9] W. Gao, S. Liang, R. Wang, Q. Jiang, Y. Zhang, Q. Zheng, B. Xie, C.Y. Toe, X. Zhu, J. Wang, Industrial carbon dioxide capture and utilization: state of the art and future challenges, Chemical Society Reviews 49(23) (2020) 8584-8686.
[10] M.J. Nobarzad, M. Tahmasebpoor, M. Heidari, C. Pevida, Theoretical and experimental study on the fluidity performance of hard-to-fluidize carbon nanotubes-based CO2 capture sorbents, Frontiers of Chemical Science and Engineering (2022).
[11] M. Iranvandi, M. Tahmasebpoor, B. Azimi, M. Heidari, C. Pevida, The novel SiO2-decorated highly robust waste-derived activated carbon with homogeneous fluidity for the CO2 capture process, Separation and Purification Technology 306 (2023) 122625.
[12] U. Kamran, S.-J. Park, Chemically modified carbonaceous adsorbents for enhanced CO2 capture: A review, Journal of Cleaner Production 290 (2021) 125776.
[13] S. Chang, Y. He, Y. Li, X. Cui, Study on the immobilization of carbonic anhydrases on geopolymer microspheres for CO2 capture, Journal of Cleaner Production 316 (2021) 128163.
[14] H. Chen, Y.J. Zhang, P.Y. He, L.C. Liu, Synthesis, characterization, and selective CO2 capture performance of a new type of activated carbon-geopolymer composite adsorbent, Journal of Cleaner Production 325 (2021) 129271.
[15] A. AlNouss, M. Shahbaz, G. McKay, T. Al-Ansari, Bio-methanol production from palm wastes steam gasification with application of CaO for CO2 capture: techno-economic-environmental analysis, Journal of Cleaner Production 341 (2022) 130849.
[16] J. Blamey, E. Anthony, J. Wang, P. Fennell, The calcium looping cycle for large-scale CO2 capture, Progress in Energy and Combustion Science 36(2) (2010) 260-279.

[17] T. Shimizu, T. Hirama, H. Hosoda, K. Kitano, M. Inagaki, K. Tejima, A twin fluid-bed reactor for removal of CO2 from combustion processes, Chemical Engineering Research and Design 77(1) (1999) 62-68.
[18] Y. Yan, K. Wang, P.T. Clough, E.J. Anthony, Developments in calcium/chemical looping and metal oxide redox cycles for high-temperature thermochemical energy storage: A review, Fuel Processing Technology 199 (2020) 106280.
[19] M. Heidari, M. Tahmasebpoor, S.B. Mousavi, C. Pevida, CO2 capture activity of a novel CaO adsorbent stabilized with (ZrO2+Al2O3+CeO2)-based additive under mild and realistic calcium looping conditions, Journal of CO2 Utilization 53 (2021) 101747.
[20] M. Heidari, M. Tahmasebpoor, A. Antzaras, A.A. Lemonidou, CO2 capture and fluidity performance of CaO-based sorbents: Effect of Zr, Al and Ce additives in tri-, bi- and mono-metallic configurations, Process Safety and Environmental Protection 144 (2020) 349-365.
[21] H. Pourpasha, S. Zeinali Heris, A. Asadi, Experimental investigation of nano-TiO2/turbine meter oil nanofluid, Journal of Thermal Analysis and Calorimetry 138(1) (2019) 57-67.
[22] H. Pourpasha, S. Zeinali Heris, Y. Mohammadfam, Comparison between multi-walled carbon nanotubes and titanium dioxide nanoparticles as additives on performance of turbine meter oil nano lubricant, Scientific Reports 11(1) (2021) 1-19.
[23] M. Kargaran, H.R. Goshayeshi, H. Pourpasha, I. Chaer, S.Z. Heris, An extensive review on the latest developments of using oscillating heat pipe on cooling of photovoltaic thermal system, Thermal Science and Engineering Progress (2022) 101489.
[24] H. Pourpasha, S.Z. Heris, M. Mohammadpourfard, The effect of TiO2 doped multi-walled carbon nanotubes synthesis on the thermophysical and heat transfer properties of transformer oil: A comprehensive experimental study, Case Studies in Thermal Engineering (2022) 102607.
[25] H. Pourpasha, S.Z. Heris, O. Mahian, S. Wongwises, The effect of multi-wall carbon nanotubes/turbine meter oil nanofluid concentration on the thermophysical properties of lubricants, Powder technology 367 (2020) 133-142.
[26] H. Pourpasha, P. Farshad, S.Z. Heris, Modeling and optimization the effective parameters of nanofluid heat transfer performance using artificial neural network and genetic algorithm method, Energy Reports 7 (2021) 8447-8464.
[27] A.V. Moghadam, H.R. Goshayeshi, I. Chaer, A. Paurine, S. Zeinali Heris, H. Pourpasha, Experimental investigation of multiwall carbon nanotubes/water nanofluid pool boiling on smooth and groove surfaces, International Journal of Energy Research 46(14) (2022) 19882-19893.
[28] H. Alizadeh, H. Pourpasha, S.Z. Heris, P. Estellé, Experimental investigation on thermal performance of covalently functionalized hydroxylated and non-covalently functionalized multi-walled carbon nanotubes/transformer oil nanofluid, Case Studies in Thermal Engineering 31 (2022) 101713.
[29] R. Javadpour, S.Z. Heris, Y. Mohammadfam, S.B. Mousavi, Optimizing the heat transfer characteristics of MWCNTs and TiO2 water-based nanofluids through a novel designed pilot-scale setup, Scientific Reports 12(1) (2022) 15154.
[30] S.B. Mousavi, S. Zeinali Heris, M.G. Hosseini, Experimental investigation of MoS2/diesel oil nanofluid thermophysical and rheological properties, International Communications in Heat and Mass Transfer 108 (2019) 104298.
[31] S.S. Seyedi, M.R. Shabgard, S.B. Mousavi, S. Zeinali Heris, The impact of SiC, Al2O3, and B2O3 abrasive particles and temperature on wear characteristics of 18Ni (300) maraging steel in abrasive flow machining (AFM), International Journal of Hydrogen Energy 46(68) (2021) 33991-34001.

[32] A. Aghaei Sarvari, S. Zeinali Heris, M. Mohammadpourfard, S.B. Mousavi, P. Estellé, Numerical investigation of TiO2 and MWCNTs turbine meter oil nanofluids: Flow and hydrodynamic properties, Fuel 320 (2022) 123943.
[33] E. Sobhani, S.Z. Heris, S.B. Mousavi, The Synergistic Effect of Intumescent Fire-Resistive Paint Containing TiO2 Nanoparticles and Chlorinated Paraffin onto Atmospheric-Metallic Substrates, ChemistrySelect 7(44) (2022) e202203513.
[34] M. Khanmohammadi, J.R. Shahrouzi, F. Rahmani, Insights into mesoporous MCM-41-supported titania decorated with CuO nanoparticles for enhanced photodegradation of tetracycline antibiotic, Environmental Science and Pollution Research 28(1) (2021) 862-879.
[35] P. Delir Kheyrollahi Nezhad, M. Haghighi, N. Jodeiri, F. Rahmani, Sol–gel preparation of NiO/ZrO2(x)–MgO(100−x) nanocatalyst used in CO2/O2 oxidative dehydrogenation of ethane to ethylene: influence of Mg/Zr ratio on catalytic performance, Journal of Sol-Gel Science and Technology 80(2) (2016) 436-450.
[36] Y. Hu, H. Lu, W. Liu, Y. Yang, H. Li, Incorporation of CaO into inert supports for enhanced CO2 capture: A review, Chemical Engineering Journal 396 (2020) 125253.
[37] H.R. Radfarnia, M.C. Iliuta, Metal oxide-stabilized calcium oxide CO2 sorbent for multicycle operation, Chemical Engineering Journal 232 (2013) 280-289.
[38] A. Antzara, E. Heracleous, A.A. Lemonidou, Improving the stability of synthetic CaO-based CO2 sorbents by structural promoters, Applied energy 156 (2015) 331-343.
[39] S.A. Nicolae, P.Á. Szilágyi, M.M. Titirici, Soft templating production of porous carbon adsorbents for CO2 and H2S capture, Carbon 169 (2020) 193-204.
[40] J. Sun, W. Liu, H. Chen, Y. Zhang, Y. Hu, W. Wang, X. Li, M. Xu, Stabilized CO2 capture performance of extruded–spheronized CaO-based pellets by microalgae templating, Proceedings of the Combustion Institute 36(3) (2017) 3977-3984.
[41] Y. Xu, H. Ding, C. Luo, Y. Zheng, Y. Xu, X. Li, Z. Zhang, C. Shen, L. Zhang, Porous spherical calcium-based sorbents prepared by a bamboo templating method for cyclic CO2 capture, Fuel 219 (2018) 94-102.
[42] V. Derevschikov, V. Semeykina, J. Bitar, E. Parkhomchuk, A. Okunev, Template technique for synthesis of CaO-based sorbents with designed macroporous structure, Microporous and Mesoporous Materials 238 (2017) 56-61.
[43] Y. Xu, H. Ding, C. Luo, Y. Zheng, Y. Xu, X. Li, Z. Zhang, C. Shen, L. Zhang, Effect of lignin, cellulose and hemicellulose on calcium looping behavior of CaO-based sorbents derived from extrusion-spherization method, Chemical Engineering Journal 334 (2018) 2520-2529.
[44] M.A. Naeem, A. Armutlulu, Q. Imtiaz, F. Donat, R. Schäublin, A. Kierzkowska, C.R. Müller, Optimization of the structural characteristics of CaO and its effective stabilization yield high-capacity CO2 sorbents, Nature communications 9(1) (2018) 1-11.
[45] A. Armutlulu, M.A. Naeem, H.J. Liu, S.M. Kim, A. Kierzkowska, A. Fedorov, C.R. Müller, Multishelled CaO microspheres stabilized by atomic layer deposition of Al2O3 for enhanced CO2 capture performance, Advanced Materials 29(41) (2017) 1702896.
[46] S.M. Kim, A. Armutlulu, A.M. Kierzkowska, C.R. Müller, Inverse opal-like, Ca3Al2O6-stabilized, CaO-based CO2 sorbent: stabilization of a highly porous structure to improve its cyclic CO2 uptake, ACS Applied Energy Materials 2(9) (2019) 6461-6471.
[47] Sol-gel synthesis and catalytic performance of Ni-Co/Al 2 O 3 -MgO-ZrO 2 nanocatalyst with different ZrO 2 -loadings used in CH 4 /CO 2 reforming for hydrogen production, International Journal of Oil, Gas and Coal Technology 8(3) (2014) 304-324.
[48] P.D.K. Nezhad, M. Haghighi, F. Rahmani, CO2/O-2-enhanced ethane dehydrogenation over a sol-gel synthesized Ni/ZrO2-MgO nanocatalyst: Effects of Mgo, ZrO (2,) and NiO on the catalytic performance, Particulate Science and Technology 36(8) (2018) 1017-1028.
[49] M. Heidari, S.B. Mousavi, F. Rahmani, P.T. Clough, S. Ozmen, The novel Carbon Nanotube-assisted development of highly porous CaZrO3-CaO xerogel with boosted sorption

activity towards high-temperature cyclic CO2 capture, Energy Conversion and Management 274 (2022) 116461.
[50] M. Broda, C.R. Müller, Sol–gel-derived, CaO-based, ZrO2-stabilized CO2 sorbents, Fuel 127 (2014) 94-100.
[51] Y. Wang, W. Zhang, R. Li, W. Duan, B. Liu, Design of Stable Cage-like CaO/CaZrO3 Hollow Spheres for CO2 Capture, Energy & Fuels 30(2) (2016) 1248-1255.
[52] H.J. Yoon, K.B. Lee, Introduction of chemically bonded zirconium oxide in CaO-based high-temperature CO2 sorbents for enhanced cyclic sorption, Chemical Engineering Journal 355 (2019) 850-857.
[53] M. Zhao, M. Bilton, A.P. Brown, A.M. Cunliffe, E. Dvininov, V. Dupont, T.P. Comyn, S.J. Milne, Durability of CaO–CaZrO3 Sorbents for High-Temperature CO2 Capture Prepared by a Wet Chemical Method, Energy & Fuels 28(2) (2014) 1275-1283.
[54] A.N. Antzara, A. Arregi, E. Heracleous, A.A. Lemonidou, In-depth evaluation of a ZrO2 promoted CaO-based CO2 sorbent in fluidized bed reactor tests, Chemical Engineering Journal 333 (2018) 697-711.
[55] M. Zhao, X. He, G. Ji, Y. Song, X. Zhao, Zirconia incorporated calcium looping absorbents with superior sintering resistance for carbon dioxide capture from in situ or ex situ processes, Sustainable Energy & Fuels 2(12) (2018) 2733-2741.
[56] H. Guo, S. Wang, C. Li, Y. Zhao, Q. Sun, X. Ma, Incorporation of Zr into calcium oxide for CO2 capture by a simple and facile sol–gel method, Industrial & Engineering Chemistry Research 55(29) (2016) 7873-7879.
[57] I. Luisetto, M.R. Mancini, L. Della Seta, R. Chierchia, G. Vanga, M.L. Grilli, S. Stendardo, CaO–CaZrO3 Mixed Oxides Prepared by Auto–Combustion for High Temperature CO2 Capture: The Effect of CaO Content on Cycle Stability, Metals 10(6) (2020) 750.
[58] X. He, G. Ji, T. Liu, M. Zhao, Effects of the Inert Materials on the Stability of Ca-Based CO2 Sorbents and the Synergy with Cement Manufacture, Energy & Fuels 33(10) (2019) 9996-10003.
[59] S.M. Hashemi, D. Karami, N. Mahinpey, Solution combustion synthesis of zirconia-stabilized calcium oxide sorbents for CO2 capture, Fuel 269 (2020) 117432.
[60] R. Koirala, K.R. Gunugunuri, S.E. Pratsinis, P.G. Smirniotis, Effect of zirconia doping on the structure and stability of CaO-based sorbents for CO2 capture during extended operating cycles, The Journal of Physical Chemistry C 115(50) (2011) 24804-24812.
[61] H.R. Radfarnia, M.C. Iliuta, Development of zirconium-stabilized calcium oxide absorbent for cyclic high-temperature CO2 capture, Industrial & engineering chemistry research 51(31) (2012) 10390-10398.
[62] S.B. Mousavi, S.Z. Heris, P. Estellé, Experimental comparison between ZnO and MoS 2 nanoparticles as additives on performance of diesel oil-based nano lubricant, Scientific reports 10(1) (2020) 1-17.
[63] S.B. Mousavi, S. Zeinali Heris, Experimental investigation of ZnO nanoparticles effects on thermophysical and tribological properties of diesel oil, International Journal of Hydrogen Energy 45(43) (2020) 23603-23614.
[64] S.B. Mousavi, S. Zeinali Heris, P. Estellé, Viscosity, tribological and physicochemical features of ZnO and MoS2 diesel oil-based nanofluids: An experimental study, Fuel 293 (2021) 120481.
[65] S.L. González-Cortés, F.E. Imbert, Fundamentals, properties and applications of solid catalysts prepared by solution combustion synthesis (SCS), Applied Catalysis A: General 452 (2013) 117-131.
[66] R. Ianoş, P. Barvinschi, Solution combustion synthesis of calcium zirconate, CaZrO3, powders, Journal of Solid State Chemistry 183(3) (2010) 491-496.

[67] Y. Chen, W. Zhou, Z. Shao, N. Xu, Nickel catalyst prepared via glycine nitrate process for partial oxidation of methane to syngas, Catalysis Communications 9(6) (2008) 1418-1425.
[68] H. Guo, J. Feng, Y. Zhao, S. Wang, X. Ma, Effect of micro-structure and oxygen vacancy on the stability of (Zr-Ce)-additive CaO-based sorbent in CO2 adsorption, Journal of CO2 Utilization 19 (2017) 165-176.
[69] S. Naghash-Hamed, N. Arsalani, S.B. Mousavi, The Catalytic Reduction of Nitroanilines Using Synthesized CuFe2O4 Nanoparticles in an Aqueous Medium, ChemistryOpen 11(11) (2022) e202200156.
[70] S. Naghash-Hamed, N. Arsalani, S.B. Mousavi, Facile copper ferrite/carbon quantum dot magnetic nanocomposite as an effective nanocatalyst for reduction of para-nitroaniline and ortho-nitroaniline, Nano Futures 6(4) (2022) 045003.
[71] F. Yan, J. Jiang, X. Chen, S. Tian, K. Li, Synthesis and characterization of silica nanoparticles preparing by low-temperature vapor-phase hydrolysis of SiCl4, Industrial & Engineering Chemistry Research 53(30) (2014) 11884-11890.
[72] F. Yan, J. Jiang, K. Li, N. Liu, X. Chen, Y. Gao, S. Tian, Green synthesis of nanosilica from coal fly ash and its stabilizing effect on CaO sorbents for CO2 capture, Environmental science & technology 51(13) (2017) 7606-7615.

Highly robust ZrO2-stabilized CaO nanoadsorbent prepared via a facile one-pot MWCNT-template method for CO2 capture under realistic calcium looping conditions

Mousavi, Seyed Borhan

2022-12-27

Mousavi SB, Heidari M, Rahmani F, et al., (2023) Highly robust Zr-stabilized CaO nanoadsorbent developed by a facile one-pot MWCNT-assistance method for CO2 capture under realistic calcium looping conditions. Journal of Cleaner Production, Volume 384, January 2023, Article number 135579

https://doi.org/10.1016/j.jclepro.2022.135579